Non-Classical Crystallisation of Dipicolinic Acid in Microemulsions

*Cen Chen, Catherine E. Nicholson, Helen E. Ramsey and Sharon J. Cooper**

Durham University, Department of Chemistry, South Road, Durham, DH1 3LE, UK

ABSTRACT

Dipicolinic acid (DPA) was crystallised in microemulsions to investigate the effect of 3D nanoconfinement on the crystallisation process. The microemulsions were acidified with 2M HCl to prevent the formation of DPA metal salts, which occurs due to a pH shift towards neutrality arising from the nanoconfinement. TEM analysis showed that 30-100 nm square-plate nanoaggregates crystallised from these acidified microemulsions. Higher resolution TEM images revealed that the nanoaggregates consisted of smaller 3-10 nm nanocrystals. The FFT's obtained from images of these nanocrystals were similar to the diffraction pattern arising from the whole nanoaggregate confirming that the nanocrystals exhibited ordered packing and resembled mesocrystals. The crystallisation of the nanoaggregates is aided by the suppression of Ostwald ripening of the nanocrystals in the nm-sized microemulsion droplets and surfactant adsorption onto the nanocrystals.

INTRODUCTION

Crystallisation and nanoparticle synthesis within microemulsions has attracted significant interest because improved control over crystal size, morphology and polymorph selection can potentially arise. Recently, we have demonstrated that a microemulsion can be used to exert thermodynamic control over the crystallisation process so that the most stable polymorph selectively crystallises under conditions where crystallisation is just favourable.[1] This methodology has been successfully adopted to produce the stable polymorphs of glycine, mefenamic acid and 5-methyl-2-[(2-nitrophenyl) amino]-3-thiophenecarbonitrile (commonly known as ROY because of its red, orange and yellow polymorphs) under conditions that would produce metastable forms in bulk solution.[1-3] However, the crystallisation of organic hydrates has yet to be studied using this methodology. Dipicolinic acid (DPA, pyridine-2,6-dicarboxylic acid), which is known to exist as an anhydrous form,[4] a monohydrate form[5] and a dihydrate form[6] under ambient conditions, was chosen as a model compound for such a study.

DPA was first isolated in 1936,[7] and is an essential part of bacterial spores.[8] DPA is a chelating agent for metal complexes and can also form hydrogen-bonded cocrystals with, for instance, caffeine[9] and urea.[10] Our initial studies into crystallisation of DPA from aqueous solution in microemulsions produced metal DPA salts rather than the free acid expected. This was considered to result from a pH shift towards neutrality in the microemulsion droplets,[11,12] which may arise from the preferential adsorption of H+ ions at the droplet interface.[12] The pH shift, combined with DPA's metal binding ability, then leads to the precipitation of salts. To prevent DPA salt formation, DPA can be dissolved in 2M HCl solutions to ensure a sufficiently acidic

environment in the microemulsion phases for the free acid to crystallise. We have found that the DPA that crystallises under these conditions has a morphology that suggests a non-classical crystal growth route, involving oriented aggregation of nanocrystals[13] rather than molecule by molecule growth.

The concept of non-classical crystallisation was described by Cölfen and Antonietti[14] as a process involving parallel, multiple nucleation events to form nanoparticles, which then aggregate to form a superstructure, in contrast to a single nucleation event producing a single crystal. The orientated attachment of the nanoparticle building units can result in either a single crystal or in a highly-organised structure, termed a mesocrystal, in which the nanocrystalline buildings blocks are nevertheless still evident. [14,15] In particular, if the nanocrystals fuse in crystallographic registry with few impurities included, a single crystal develops, and evidence for the individual nanocrystalline building blocks characteristic of the non-classical crystallisation route, can be lost. In contrast, if the nanocrystals remain separated by disordered layers, the final structure is a mesocrystal, in which the nanocrystalline building blocks are still discernible.

Mesocrystals are usually transient and kinetically metastable, with single crystals being the final product. Nevertheless, mesocrystal formation has been reported for a wide range of materials, including biominerals[16,17] (e.g. sea urchins[18] and hydroxyapatite[19,20]) and metal complexes (e.g. CuO[21] and V_2O_5[22]), but only a few organic compounds (e.g. DL-alanine[23,24]). Although the synthesis of metal and inorganic nanoparticles from microemulsions is well-established,[25-27] the formation of organic nanocrystals from microemulsions has been less well-documented.[28] Here we report the formation of mesocrystal-like structures of size ~30-100 nm arising from the oriented aggregation of DPA nanocrystals in microemulsions, and suggest a

possible formation mechanism. To our knowledge, this is the first time oriented nanoaggregates of an organic molecule have been grown from microemulsions.

EXPERIMENTAL SECTION

Microemulsion preparation. The surfactant systems adopted in this study were Triton X-100/1-hexanol (w/w 2.2:1) and Triton X-114. The surfactants, Triton X-100 (polyoxyethylene *tert*-octylphenyl ether, $C_{14}H_{22}O(C_2H_4O)_n$, n~9.5) and Triton X-114 (polyoxyethylene *tert*-octylphenyl ether, $C_{14}H_{22}O(C_2H_4O)_n$, n~7.5) and cosurfactant 1-hexanol were purchased from Sigma-Aldrich and used without further purification. Cyclohexane was used as the continuous phase, with the ratio of surfactant(s) to cyclohexane maintained at 1.2: 1 and 0.43: 1 w/w for Triton X-100/1-hexanol and Triton X-114, respectively. The dispersed phase was prepared by dissolving either 18 mg ml^{-1} or 12 mg ml^{-1} of anhydrous DPA solid (99%, Sigma-Aldrich) in 2.0 M HCl solution. The volume of dispersed phase was 225 µl and 65 µl of DPA solution per gram of the combined surfactant and continuous phase for Triton X-100 and X-114, respectively, corresponding to dispersed phase volumes fractions of 16% for the Triton X-100/1-hexanol and 5% for the Triton X-114 microemulsions. Microemulsions were prepared by mixing the required components and were then shaken manually (Triton X-100/1-hexanol) or sonicated in a 20 °C water bath for 10-20 minutes (Triton X-114) to obtain a transparent single phase. The microemulsion samples were then left at 4 °C to induce crystallisation.

SAXS measurements. SAXS measurements were performed on a Bruker Nanostar SAXS instrument, with cross coupled Gδbel mirrors and pin-hole collimation for point focus geometry. The sealed-tube X-ray source was operated at 40 kV and 35 mA to produce Cu Kα radiation of wavelength 1.54 Å. The SAXS camera was fitted with a Hi-star 2D detector with an effective

pixel size of 100 μm. Microemulsion samples were contained in 2 mm quartz capillaries. The optics and sample chamber were under vacuum to minimise air scatter. The scattering data collected was analysed using GADDS software. The background scattering from the solvent is subtracted and the scattering pattern of the sample is integrated to give the one-dimensional scattering intensity function $I(q)$. q is the length of the scattering vector, defined by $q = (4\pi/\lambda)\sin\theta$, with λ being the wavelength and 2θ the scattering angle. The sample to detector distance was chosen to be 650 mm, providing a q range of 0.3 to 3.2 nm^{-1}. The collection time was 8 hours.

SAXS GIFT analysis. In GIFT analysis,[29] the scattering intensity $I(q)$ is related to the product of the form factor $P(q)$ and the structure factor $S(q)$ arising from intra- and interparticle scattering, respectively: $I(q) \propto nP(q)S(q)$, where n is the number density of particles. $P(q)$ is given by the Fourier transformation of the pair-distance distribution function, $p(r)$:

$$P(q) = 4\pi \int_0^\infty p(r) \frac{sin(qr)}{qr} dr$$

The $p(r)$ function gives the frequency of occurrence of vectors of length r, weighted by the electron density at either end of the vector. $p(r)$ contains essential information about the size and shape of the scattering particles, without additional hypothesis.

$S(q)$ describes the spatial distribution of the particles and is related to the pair-correlation function $g(r)$ by:

$$S(q) = 1 + 4\pi n \int_0^\infty [g(r) - 1] \frac{\sin(qr)}{qr} r^2 \, dr$$

GIFT analysis was used to obtain the pair distance distribution function $p(r)$ and a mean droplet size, r, of the microemulsions by employing a hard sphere structure factor to account for the interparticle interactions. A Porod extrapolation was first undertaken on the SAXS data, with this residual background then subtracted from the scattering intensity function $I(q)$. The subtraction of the residual background ensures the $p(r)$ function has a value ≈ 0 at $r = 0$ but has little effect on the distribution at larger distances, and the determined droplet sizes.[30]

TEM. No macroscopic crystals were observed with the microemulsions within 6 months. Consequently, aliquots of the microemulsions were examined using TEM. To prepare the TEM sample, drops of the microemulsions were first deposited onto a holey carbon grid, left to partially dry and then rinsed with cyclohexane. The TEM grids were examined in a JEOL 2100F Schottky field emission gun TEM (FEG TEM) operating at 200 kV. Phase contrast, high resolution electron microscopy (HREM) and diffraction patterns (DP) were imaged by a Gatan Orius Camera and revealed the presence of nanometer-size crystals. Digital Micrograph® platform software was used to capture the images and to perform further analysis, including generating the Fast-Fourier transform (FFT) images of a selected area. The structure of an individual nanocrystal was determined by indexing the FFT extracted from the appropriate region of the image. A determination of the chemical composition of the sample was performed using an Oxford INCAx-Sight Si(Li) detector for Energy-dispersive X-ray spectroscopy (EDX).

RESULTS AND DISCUSSION

The Triton X-100/1-hexanol and Triton X-114 microemulsions were relatively viscous (~30 and 35 cps, respectively), reflecting the viscosities of the liquid Triton X-100 and Triton X-114

surfactants (~240 cps and 260 cps, respectively) and their large volume fractions (0.26 and 0.23, respectively). The formation of lyotropic liquid crystal phases could be ruled out, given the absence of sharp and higher order SAXS peaks and the lack of birefringence when the samples were viewed through cross polarisers. The SAXS scattering curve of $I(q)$ vs. q for the Triton X-100/1-hexanol and Triton X-114 microemulsions with DPA (Figure 1) were similar to those obtained without DPA (Supporting Information Figure S1) showing that the DPA did not have a significant effect on the average microemulsion structure. The SAXS scattering curve of $I(q)$ vs. q for the Triton X-100/1-hexanol microemulsions show a single broad peak at $q \approx 0.8$ nm^{-1} (Figure 1a and Supporting Information Figure S1a), whereas for the Triton X-114 microemulsions with and without DPA, a slight shoulder at $q \approx 0.5$ nm^{-1} is evident (Figure 1c and Supporting Information Figure S1c); both features are common for microemulsion samples and can arise from either a droplet or bicontinuous structure. However, the absence of Winsor III systems when excess oil and water are added to the microemulsions suggests that a bicontinuous structure is not formed; instead an excess water phase developed below the microemulsion consistent with the Winsor II water-in-oil microemulsion system. A water-in-oil droplet structure would also be expected from the relatively low dispersed phase volume fractions. Consequently, the scattering curves were analysed using GIFT analysis[29] assuming a monodisperse droplet structure.

The pair-distance distribution function $p(r)$ vs r curves obtained from GIFT analysis on the $I(q)$ vs. q curves for the Triton X-100/1-hexanol and Triton X-114 microemulsions with DPA show a single maximum typical of homogeneous particles (Figure 1b and Figure 1d). This suggests that the hydrophobic shell region of the microemulsion droplets have an electron density contrast sufficiently similar to the surrounding cyclohexane continuous phase that the scattering arises

mainly from the hydrophilic core of the microemulsion droplets. The approximately symmetrical shape of the $p(r)$ curves show that the droplets are approximately spherical. R_g values of 2.3 nm and 2.7 nm were obtained from the GIFT analysis for the DPA Triton X-100/1-hexanol and Triton X-114 microemulsions, respectively. Hence, assuming a spherical geometry, this gives mean hydrophilic core radii of ≈3.0 nm and ≈3.5 nm for the DPA Triton X-100/1-hexanol and Triton X-114 microemulsions, respectively. Note the mean diameter of the hydrophillic cores is also given by the point at which $p(r)$ drops to zero, corresponding to ≈6.4 nm for the Triton X-100/1-hexanol microemulsions, in good agreement with the values obtained from the calculated R_g values. For the Triton X-114 microemulsions, $p(r)$ drops to zero at ≈8.0 nm, which is larger than the mean diameter value of 7.0 nm obtained from R_g, suggesting the tailgroups may make a small contribution to the scattering in this system. The form factor for a sphere gives a minimum $I(q)$ at $q_{min} \approx 4.48/r$, corresponding to ≈1.1 nm^{-1} and ≈1 nm^{-1} for the Triton X-100/1-hexanol and Triton X-114 microemulsions, respectively, though this feature is obscured in our data by the polydispersity of the spheres and the dominating structure factor. The q_{max} peak and shoulder positions observed in the $I(q)$ vs. q curves give an estimate of the mean interdroplet spacing, $d \sim 2\pi/q_{max}$, which corresponds to ~8 nm and ~13 nm for the Triton X-100/1-hexanol and Triton X-114 microemulsions, respectively, because the intensity $I(q)$ can be related to the product $P(q)S(q)$, with $P(q)$ monotonically decreasing in this q region, whereas $S(q)$ is peaked at $\sim 2\pi/d$.

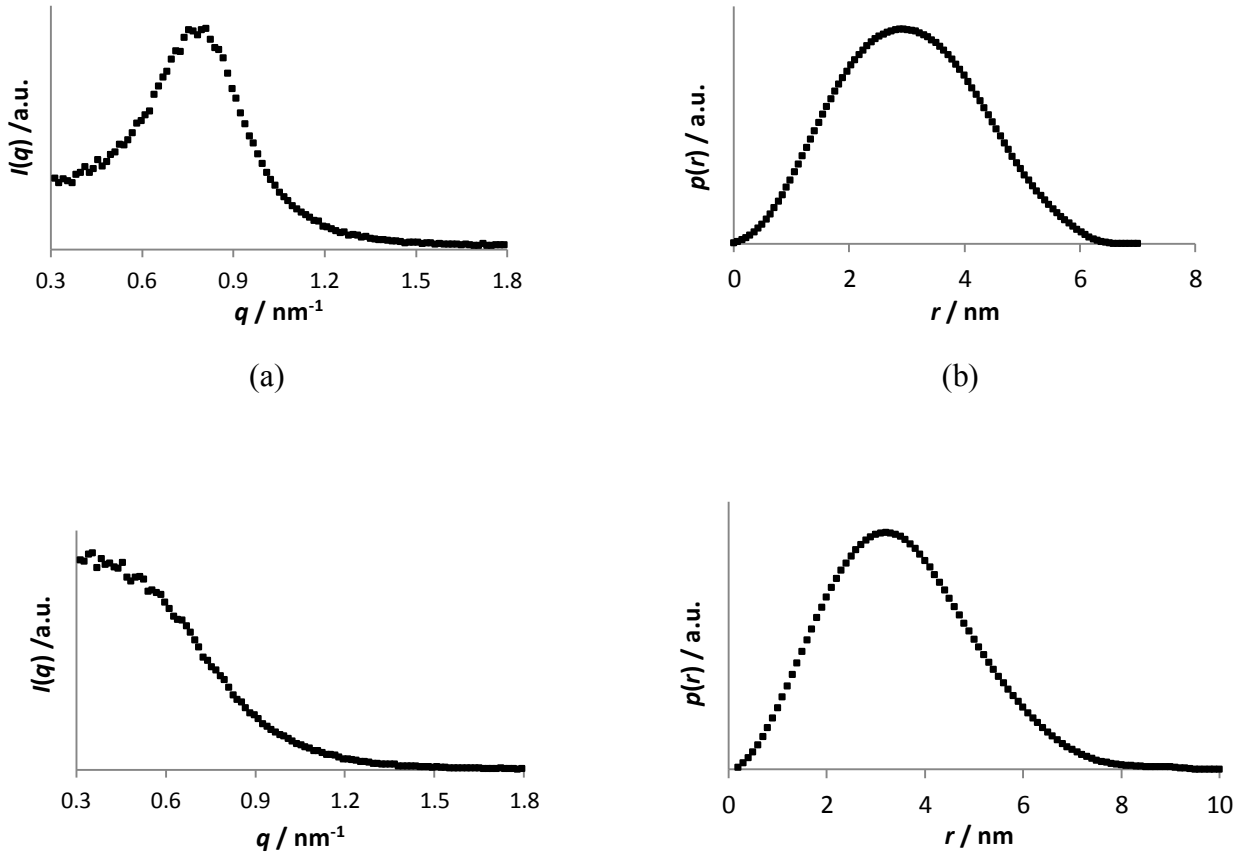

Figure 1. SAXS analysis of the microemulsions. Scattering intensity $I(q)$ vs. q for (a) the Triton X-100/1-hexanol microemulsions containing 12 mg ml^{-1} DPA in 2 M HCl and (c) the Triton X-1114 microemulsions containing 12 mg ml^{-1} DPA in 2 M HCl. Pair-distance distribution function $p(r)$ vs. r curves for (b) the Triton X-100/1-hexanol microemulsions containing 12 mg ml^{-1} DPA in 2 M HCl and (d) the Triton X-1114 microemulsions containing 12 mg ml^{-1} DPA in 2 M HCl.

The solubility of DPA in the microemulsions was determined from the quantities of DPA monohydrate that dissolved in microemulsions held at 4 °C for 1 month. In the Triton X-100/1-hexanol microemulsions, DPA has a significantly increased solubility compared to bulk aqueous solutions. At 4 °C, the solubility of DPA in the Triton X-100/1-hexanol microemulsions was 9.4 mg DPA per ml of 2 M HCl compared to only 3.1 mg per ml of 2 M HCl for the Triton X-114 microemulsions, which did not have added 1-hexanol. DPA has a solubility in hexanol of ≈3 mg ml^{-1} at 4 °C, which is similar to its value of ≈2.5 mg ml^{-1} in water at 4 °C. Consequently, the enhanced DPA solubility in the Triton X-100/1-hexanol microemulsions arises because the high interfacial concentration of 1-hexanol results in DPA residing to a significant extent within this interfacial region. The Triton X-100/1-hexanol and Triton X-114 microemulsions with 12 mg ml^{-1} DPA in the aqueous phase had mean relative supersaturations of 1.3 and 3.9, respectively, at 4 °C whilst the 18 mg ml^{-1} DPA Triton X-100/1-hexanol microemulsion had a mean relative supersaturation of 1.9. Despite these mean supersaturation levels, macroscopic-sized crystals were not produced even after 6 months. In comparison, bulk DPA solutions at this temperature and supersaturation ratio crystallised within hours and by varying the pH and solvents could be used to produce anhydrous, monohydrate and dihydrate forms (Supporting Information Figures S2, S4 and Table 1). DPA aqueous solutions in Triton X100/1-hexanol microemulsions without the added 2M HCl crystallised in a few days and gave sodium DPA salts (Supporting Information Figures S3 and S5). To further investigate the lack of macroscopic DPA crystals in DPA microemulsions with added 2M HCl, TEM was employed to visualise the samples at the nanometre scale.

Square-shaped nanoaggregates of ~30–100 nm were observed using TEM analysis for Triton X-100/1-hexanol microemulsions using 18 mg ml^{-1} (Figure 2) and 12 mg ml^{-1} (Supporting

Information Figure S6) of DPA in 2.0 M HCl solution; each nanoaggregate was composed of square or disc-shaped crystalline subunits of size ~3–10 nm. Although the HREM images indicated regions of different electron densities, both the FFT and the selected area DPs revealed single crystal-like properties; aggregates of nanocrystals are typically unorientated and so polycrystalline, whereas these nanoaggregates have similar features to mesocrystals. The nanoaggregates were considered to be of DPA monohydrate, given their DPs and FFT's (Figures 2c, d and S2b, c) showed good agreement with the [102] zone axis of the DPA monohydrate and lacked agreement with the zone axes of anhydrous DPA and DPA dihydrate. We can rule out the occurrence of DPA chlorides and DPA metal salts because only trace amounts of chlorine and metal were found in the EDX spectra (Supporting Information Figure S7).

The faces exposed in the DPA nanoaggregates grown from the Triton X-100/1-hexanol microemulsions are shown in Figure 3a, with the accompanying DP of the nanoaggregate indexed in Figure 3b. The slowest growing face with the largest exposed area was the (101), with the other two faces being the (010) and $(\bar{2}01)$. The (101) plane maintains the integrity of the DPA monohydrate hydrogen-bonded dimer and exposes water molecules and the CH groups on the pyridine ring (Figure 3c). Consequently, it might be expected that this would be a slow growing face with a lower attachment energy compared to the (010) and $(\bar{2}01)$ faces that expose the carboxylic acid hydrogen-bonding groups. Furthermore, the Triton surfactants adsorb strongly onto the (101) face. In particular, it was found that DPA grown from bulk aqueous solutions containing Triton X-100/1-hexanol crystallised as thinner plates with larger (101) faces (Figure 4c, d) compared to the morphology obtained by crystallising from bulk aqueous solution alone (Figure 4a, b). The same morphology change occurred when DPA was crystallised from bulk 0.5 M HCl solutions containing Triton X-100/1-hexanol. However, at HCl concentrations of 0.75 M,

crystallisation of mainly anhydrous DPA was observed, with the DPA monohydrate present as the minority phase, whilst at concentrations of ≥ 1 M HCl, only the anhydrous DPA form crystallised, both with and without added Triton surfactant. The lack of the monohydrate form crystallising from bulk solution at lower pH highlights that the microemulsions can produce the thermodynamically most stable monohydrate form of DPA even when a kinetic form crystallises from the analogous bulk solution.[1-3]

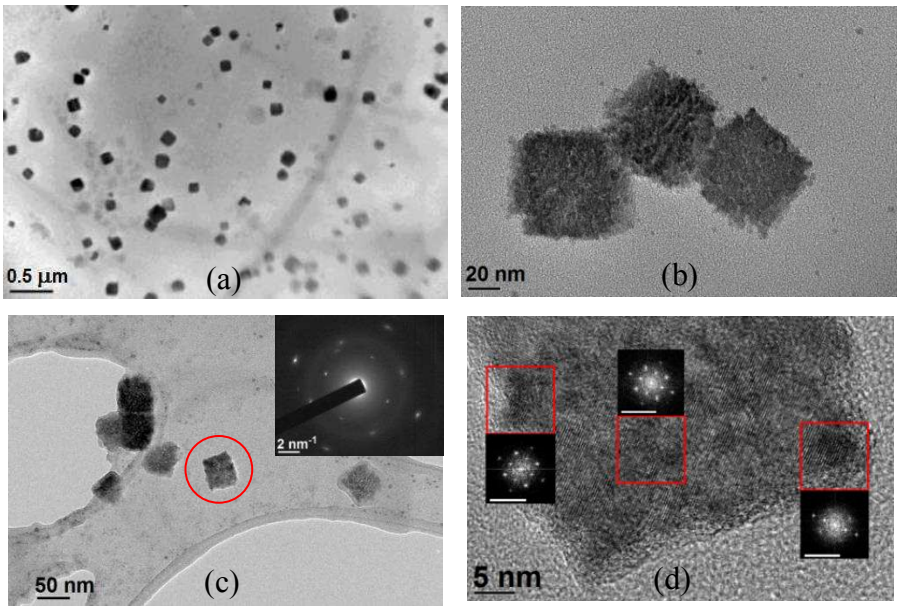

Figure 2. Representative TEM images of the DPA nanocrystals grown from the Triton X-100/1-hexanol microemulsions using 18 mg ml^{-1} DPA in 2 M HCl. The inset in (c) shows the diffraction pattern of the red circled nanoaggregate. (d) shows a high resolution image of part of the nanoaggregate circled in (c). The red-square regions in (d) show the areas from which the adjacent FFT's were produced. The white scale bars in (d) represents 10 nm^{-1}. Note the diffraction pattern in (c) and the FFT's in (d) show similar patterns and can be indexed on the DPA monohydrate [102] zone axis.

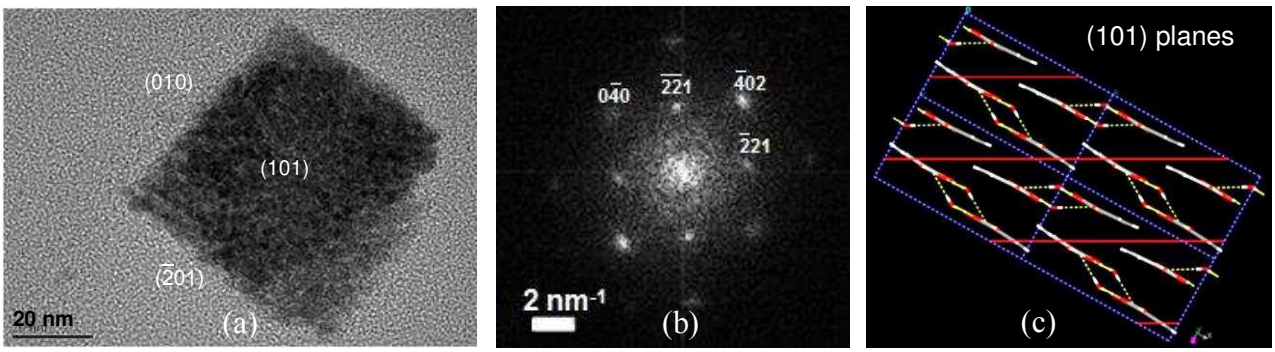

Figure 3. (a) TEM image of a typical DPA monohydrate nanoaggregate grown from the Triton X-100/1-hexanol microemulsions with the Miller indices of the faces indicated. (b) Diffraction pattern of (a) showing the [102] DPA monohydrate zone axis. (c) View down the DPA monohydrate crystal *b*-axis generated in Cerius2®.[31] Carbon atoms are depicted in gray; oxygen atoms in red, hydrogen atoms in white and hydrogen bonds are shown by dotted yellow lines. Note the integrity of the hydrogen-bonded dimers are preserved when cutting though the (101) planes shown in red.

For the Triton X-114 microemulsion samples, the DPA nanocrystals observed in the TEM were also of the monohydrate form (Supporting Information Figure S8) and consisted of nanocrystals of size ~5-10 nm with similar orientation to the DPA nanoaggregates obtained from Triton X-100/1-hexanol microemulsions. In the Triton X-114 case, however, the aggregates tended to be of poorer organisation, so that although the individual nanoparticles were more distinct, the FFTs showed more arcing (Figure 5).

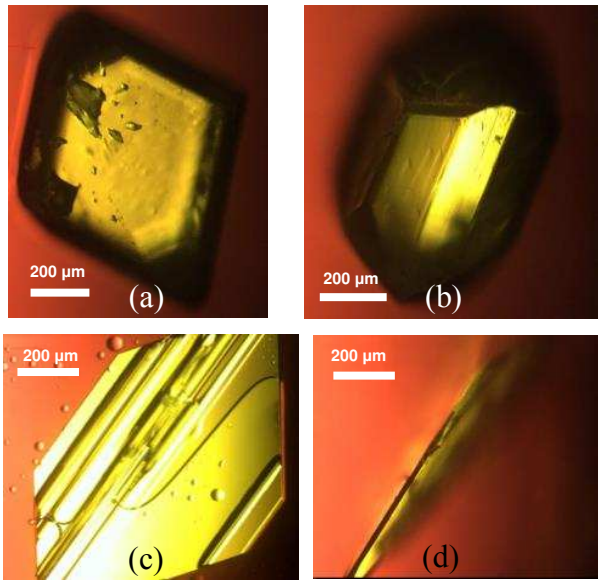

Figure 4. Optical micrographs showing the typical morphology of DPA monohydrate crystals grown from bulk aqueous solution without additives ((a) and (b)), and with added Triton X-100 and 1-hexanol ((c) and (d)). (a) and (c) are top views showing the (101) faces; (b) and (d) are side views. The images were obtained under crossed polarisers with a red tint plate inserted.

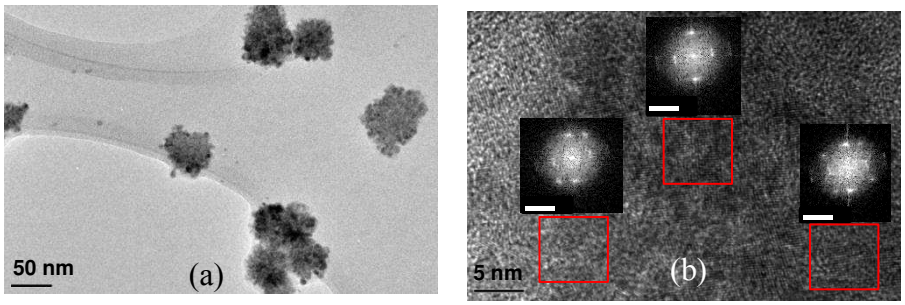

Figure 5. Representative TEM images of the DPA nanocrystals grown from the Triton X-1114 microemulsions using 12 mg ml^{-1} DPA in 2 M HCl. The insets in (b) show the FFT's of the adjacent red-boxed region. The white scale bars represent 5 nm^{-1}.

The ~3-10 nm nanocrystalline DPA building units are comparable to the microemulsions' mean droplet diameters of ~8-10 nm. This suggests that the nanocrystals nucleated and grew in individual droplets prior to the oriented aggregation process. The mean number of DPA molecules per droplet is ≈3 to 4 for all the microemulsions studied. However, due to the microemulsion polydispersity, the (assumed Poisson) variation in the distribution of solute molecules amongst droplets, and the substantial decrease in the supersaturation within a droplet as a DPA nucleus grows, only the larger and higher DPA concentration microemulsion droplets will contain sufficient DPA molecules to form the (near) stable DPA nuclei, which can then grow to ~3-10 nm in size by material exchange with other droplets during transient dimer formation. The relatively uniform size of the nanocrystals seen within each oriented nanoaggregate suggests that this nanocrystal growth proceeded at a faster rate than the nanocrystal aggregation process, until further growth of the nanocrystals was limited by the physical constraint of the microemulsion droplet size. The oriented aggregation of these nanocrystals would be expected to occur after transient droplet dimer formation between droplets each containing a nanocrystal (or nanoaggregate); the two droplets fuse, allowing the nanocrystals to diffuse to one another and then aggregate. This process will continue, ultimately producing nanoaggregates that are significantly larger than the mean droplet size. In addition, if the nanocrystals are expelled from the droplets (most likely still retaining an aqueous surfactant surrounding layer, rather than being dispersed as bare particles in the cyclohexane continuous phase), nanoaggregate formation and growth may also arise from colliding nanocrystals/nanoaggregates, or a collision between a droplet and nanocrystal/nanoaggregate.

The stronger adsorption of the surfactant onto the (101) face impedes aggregation on this face compared to the (010) and ($\bar{2}$01) faces so that thin square plate nanoaggregates of ~30-100 nm^2

ultimately develop. Nevertheless it is apparent from the high resolution TEM images showing thinner edges and thicker central portions for the nanoaggregates (Figures 2d, 6b and 6c) that the nanocrystals do stack to a limited extent upon their (101) faces. Nanocrystals attaching onto the (010) and ($\bar{2}$01) faces do so via stronger hydrogen bonding and are more likely to fuse in crystallographic registry, so that the outline of the primary nanocrystal units is less distinct, except where the attachment is less perfect, as in the Triton X-114 microemulsions. TEM images taken on samples 2 days and 1 year after the microemulsions were prepared show the oriented nanoaggregates can form within 48 hours and remain stable in the microemulsions for extended periods of time (Figure 6).

Crystallisation in microemulsions differs fundamentally from crystallisation in bulk solution. First, the environment is more varied, not only from the coexistence of hydrophobic and hydrophilic regions but also because the microemulsions can support a large range of supersaturations for limited periods of time. Secondly, the significant supersaturation depletion that occurs when a nucleus starts to grow in a droplet means that thermodynamic control of crystallisation is possible,[1-3] shown here by the crystallisation of the stable monohydrate from the microemulsions compared to the metastable anhydrous form from bulk ≥1 M HCl solutions. Thirdly, the droplet confinement significantly slows the crystallisation. Fourthly, Ostwald ripening, the growth of larger crystals and concomitant dissolution of smaller ones when the crystals are bathed in the same supersaturated solution, is more limited because the different-sized crystals are in separate microemulsion droplets the majority of the time. The nanoconfinement in microemulsions is therefore likely to aid a nanoaggregation mechanism by allowing a significant population of nanocrystals to develop in separate droplets with little dissolution from Ostwald ripening. In addition, surfactant adsorption on the nanocrystals will

also hinder dissolution. Nanocrystal aggregation may then lead to either a single crystal that is essentially indistinguishable from one grown purely by molecule by molecule addition if the aggregates fuse in crystallographic registry, or a mesocrystal or polycrystalline product may arise if the organisation is less perfect. Mesocrystals or polycrystalline aggregates would be more likely to form when surfactant is strongly adsorbed onto the nanocrystals, since this can become trapped between the aggregating nanocrystals.

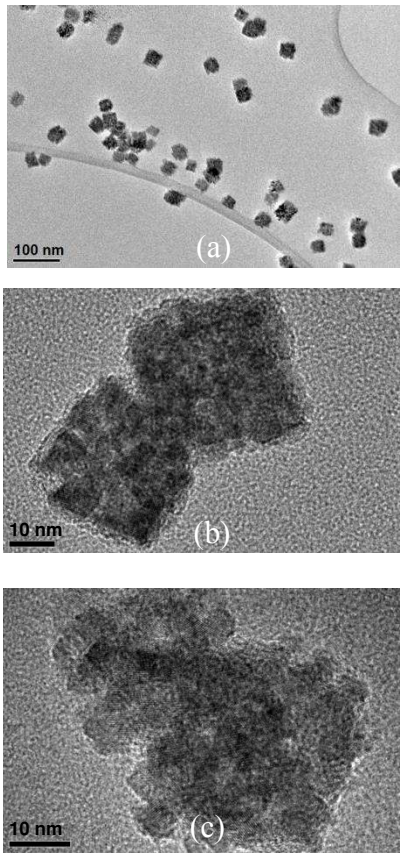

Figure 6. Representative TEM images of the DPA monohydrate nanocrystals grown and left for 1 year in the Triton X-100/1-hexanol microemulsions containing 18 mg ml^{-1} DPA in 2 M HCl.

It is not possible to ascertain the main cause of the improved nanoaggregate ordering in the Triton X-100/1-hexanol microemulsion system compared to that of the Triton X114, given the microemulsions have different compositions, viscosities, droplet sizes, supersaturations and dispersed phase volume fractions. Nevertheless, the 1-hexanol cosurfactant is likely to have two significant effects: increasing the solubility of DPA in the interfacial region and increasing the fluidity of the interfacial film.[26,27]

CONCLUSIONS

Crystallisation of DPA in Triton X-100/1-hexanol microemulsions resulted in nanoaggregates of size ~30-100 nm of DPA monohydrate via orientated attachment of primary nanocrystals of size 3–10 nm. The diffraction patterns and the FFT images of the nanoaggreagtes were single-crystal like, showing the nanoaggregates were similar to mesocrystals. In contrast, the nanoaggregates of DPA monohydrate that crystallised in the Triton X-114 microemulsions were less organised and occasionally polycrystalline, so that single-crystal like diffraction patterns were not obtained. However, the individual 5–10 nm primary building particles were more distinct compared to the Triton X-100/1-hexanol system due to their less organised packing. Although the precise mechanism leading to the oriented aggregation process requires further study, the formation of the primary 3-10 nm DPA monohydrate nanocrystals is likely to occur first, followed by a slower aggregation process. The preservation of the 3-10 nm nanocrystals is aided by both the suppression of Ostwald ripening in the microemulsions and surfactant adsorption onto the particles.

ASSOCIATED CONTENT

Supporting Information. Figures S1 to S8 and Table S1. This material is available free of charge via the Internet at http://pubs.acs.org.

AUTHOR INFORMATION

Corresponding Author *E-mail: sharon.cooper@durham.ac.uk. Tel: +44 (0) 334 2098. Fax: +44 (0) 334 2051.

Notes

The authors declare no competing financial interest.

ACKNOWLEDGMENTS

This work was supported by the UK Engineering and Physical Sciences Research Council. We thank Dr. Mendis for TEM assistance.

REFERENCES

1) Nicholson, C. E.; Chen, C.; Mendis, B.; Cooper, S. J. *Cryst. Growth Des*. **2011**, *11*, 363-366.

2) Chen, C.; Cook, O.; Nicholson, C. E.; Cooper, S. J. *Cryst. Growth Des.* **2011**, *11*, 2228-2237.

3) Nicholson, C. E.; Cooper, S. J. *Crystals* **2011**, *1*, 195-205.

4) Carranza Tellez, V.; Sanchez Gaytan, B.; Bernes, S.; Gonzalez Vergara, E. *Acta Crystallogr C* **2002**, *58*, 228-230.

5) Takusagawa, F.; Hirotsu, F.; Shimada, A. *Bull. Chem. Soc. Jpn.* **1973**, *46*, 2020-2027.

6) Grossel, M. C.; Dwyer, A. N.; Hursthouse, M. B.; Orton, J. B. *CrystEngComm*. **2007**, *9*, 207-210.

7) Udo, S. *J. Agr. Chem. Soc. Jpn.* **1936**, *12*, 386-394.

8) Edgecombe, K. E.; Weaver, D. F.; Smith-Jr, V. H. *Can. J. Chem.* **1994**, *72*, 1388-1403.

9) Das, B.; Baruah, J. B. *Cryst. Growth Des*. **2011**, *11*, 278-286.

10) Smith, G.; Baldry, K. E.; Byriel, K. A.; Kennard, C. H. L. *Aust. J. Chem.* **1997**, *50*, 727-736.

11) Levinger, N. E.; Rubenstrunk, L. C.; Baruah, B.; Crans, D. C. *J. Am. Chem. Soc*. **2011**, *133*, 7205–7214.

12) Crans, D. C.; Levinger, N. E. *Acc. Chem. Res.* **2012**, *45*, 1637-1645.

13) Wang, F.; Richards, V. N.; Shields, S. P.; Buhro, W. E. *Chem. Mater*. **2014**, *26*, 5−21.

14) H. Cöelfen and M. Antonietti, *Mesocrystals and nonclassical crystallization*, John Wiley & Sons Ltd, Chichester, 2008.

15) Song, R.-Q.; Cölfen H. *Adv. Mater*. **2010**, *22*, 1301–1330.

16) Page M. G.; Cölfen, H. *Cryst. Growth Des*. **2006**, *6*, 1915-1920.

17) Wang, T.; Cölfen H.; Antonietti, M. *J. Am. Chem. Soc.* **2005**, *127*, 3246-3247.

18) Seto, J.; Ma, Y.; Davis, S. A.; Meldrum, F.; Gourrier, A.; Kim, Y.-Y.; Schilde, U.; Sztucki, M.; Burghammer, M.; Maltsev, S.; Jäger C.; H. Cölfen, H. *P. Natl. Acad. Sci. USA* **2012**, *109*, 3699-3704.

19) Cai Y. Tang, R. *J. Mater. Chem.* **2008**, *18*, 3775-3787.

20) Tao, J.; Pan, H.; Zeng, Y.; Xu, X.; Tang, R. *J. Phys. Chem. B* **2007**, *111*, 13410-13418.

21) Sun, S.; Zhang, X.; Zhang, J.; Wang, L.; Song, X.; Yang, Z. *CrystEngComm*. **2013**, *15*, 867-877.

22) Lausser, C.; Cölfen H.; Antonietti, M. *ACS Nano* **2011**, *5*, 107-114.

23) Wohlrab, S.; Pinna, N.; Antonietti, M.; Cölfen, H. *Chem. Eur. J.* **2005**, *11*, 2903 – 2913.

24) Ma, Y.; Cölfen, H.; Antonietti, M. *J. Phys. Chem. B* **2006,** *110,* 10822-10828.

25) Ganguli, A. K.; Ganguly, A.; Vaidya, S. *Chem. Soc. Rev*. **2010**, *39*, 474-485.

26) Eastoe, J.; Hollamby, M. J.; Hudson, L. Adv. Colloid Interface Sci. **2006**, 128-130, 5-15.

27) López-Quintela, M. A.; Tojo, C.; Blanco, M. C.; Garćia Rio, L. G.; Leis, J. R. *Curr. Opin. Colloid Interface Sci*. **2004**, *9*, 264–278.

28) Margulis-Goshen, K.; Magdassi, S. Curr. Opin. Colloid Interface Sci. **2012**, 17, 290–296.

29) Brunner-Popela, J.; Glatter, O. *J. Appl. Cryst.* **1997**, *30*, 431-442.

30) Glatter, O.; Kratky, O. *Small Angle X-ray Scattering*. (Academic Press, London, 1982).

31) B. M. S. Inc, *Cerius2 Version 3.8* BIOSYM/Molecular Simulations, 1998.